Polymer Testing 84 (2020) 106389

Contents lists available at ScienceDirect

Polymer Testing

journal homepage: http://www.elsevier.com/locate/polytest

Property Modelling

A new viscoplastic model and experimental characterization for thermosetting resins

Ehsan Shafiei, Mehdi Saeed Kiasat *

Department of Maritime Engineering, Amirkabir University of Technology, Hafez Ave 424, Tehran, Iran

ARTICLE INFO

Keywords:
Viscoplastic model
Rate-dependency
Thermosetting resins

ABSTRACT

Resins as matrix materials for structural composites show nonlinear rate-dependent mechanical behaviors. In the present work, a new viscoplastic constitutive equation based on a potential function is proposed to predict the mechanical response of an epoxy matrix to any three-dimensional loading condition. The proposed potential function is a combination of the second and third invariants of the deviatoric stress tensor as well as the first invariant of the stress tensor, i.e. the hydrostatic stress. Series of tensile and shear constant-rate straining tests were performed on epoxy resin specimens up to the fracture. Under shear loading, the nonlinearity of the stress-strain curve and the rate dependency of the initial modulus and strength are more significant than that under tensile loading. The viscoplastic model parameters are derived from the experimental data, and the fracture patterns of the specimens under tensile and shear loadings are studied. Further, the model predictions are compared with a known rate-dependent model to show the accuracy of the presented model.

1. Introduction

Thermosetting resin based fiber-reinforced composites are structural materials used in many applications subjected to different loading conditions. Dynamic loading conditions from very low to very high loading rates, may introduce different responses by the polymeric composite material. The mechanical response of a composite material is governed by the mechanical behaviors of its constituents including the reinforcing fibers and the thermosetting resin matrix. Structural synthetic fibers mostly behave nearly elastic and according to the fiber type, may negligibly depend on the loading rate. However, the significant rate-dependent plastic mechanical behavior of the resin matrix causes the substantial viscoplastic behavior of the composite material.

Experimental rate-dependent characterizations on various types of fiber-reinforced resins are reported in the literature. Straining rates from quasi-static about 10^{-4} 1/s to very high rates about 100 1/s have been considered for material characterization. Carbon/epoxy composites behave linearly in the longitudinal direction and their initial modulus show almost no rate dependency [1]. On the other hand, although the longitudinal response of glass/epoxy unidirectional composites under different strain rates are linear [2,3], their modulus and strength were observed to increase by 8.5% [4] and 45% [5], respectively. In off-axis loading conditions, composites demonstrate more nonlinear and rate sensitive stiffness and strength [6,7].

The tensile strength and modulus of carbon/epoxy unidirectional plies in transverse direction show an increase of 17.8% and 12.5%, respectively, for increasing the strain rate from 1.04×10^{-4} 1/s to 100 1/s [1]. Also for the same strain rates, a drastic increase of the shear strength and modulus to about 77.5% and 77.1% were reported for carbon/epoxy laminates [1]. Among off-axis angles, 45° condition manifested specifically higher degree of nonlinearity and rate dependency [2,3,8] due to the dominant resin nonlinear behavior. Experimental data for woven fabric composites [9,10] and off-axis loading conditions [11–13] confirmed significant nonlinear rate-dependency of the stiffness and strength.

Experimental observations have proved the effects of strain rate on tensile and shear responses of epoxy polymer matrices. An increase of about 35% was observed for the ultimate tensile strength of an epoxy with increasing the strain rate from 10 1/s to 10^5 1/s [14]. Farrokh and Khan [15] investigated the rate dependency of the polymer Nylon 101 subjected to tensile and torsional load conditions. They reported that the ultimate tensile and shear strength increase about 30% and 36% for the increase of the strain rate from 10^{-5} to 1 1/s. The intrinsic effect of the hydrostatic stress on the plastic deformation of polymers was later on emphasized. Shin and Pae [16] investigated the effects of hydrostatic pressure on the shear behavior of an epoxy resin. Also, creep tests [17]

* Corresponding author.
E-mail address: kiasat@aut.ac.ir (M.S. Kiasat).

https://doi.org/10.1016/j.polymertesting.2020.106389
Received 6 October 2019; Received in revised form 22 January 2020; Accepted 29 January 2020
Available online 31 January 2020

and DMA tests [18] have clearly showed the inherent time dependency of all mechanical properties of epoxy compounds.

In order to determine the contribution of the polymeric matrix in the nonlinear behavior of the composite, several plastic rate-sensitive constitutive equations have been developed for polymers [19,20]. Early constitutive equations were based on the second invariant of the deviatoric stress to obtain the plastic deformation. Drucker and Prager [21] presented a yield function including the first invariant of stress in addition to the second invariant of deviatoric stress. In the literature, stress-based potential functions involving the hydrostatic stress and the second invariant of the deviatoric stress have been used to derive not only the plastic deformation [5,15] but also the viscoplastic deformation [22–24]. Werner et al. [19] modified the Drucker–Prager yield criterion to develop a strain-based potential function able to account for the sign of strain and the coupling of volumetric and deviatoric deformations. Goldberg and Stouffer [23] modified a viscoplastic model using a potential function to analyze the rate-dependent behavior of polymeric materials.

According to the literature, the main reason for the nonlinear and rate-dependent behavior of a composite material is due to its polymeric matrix. In the present work, a new viscoplastic constitutive equation based on a potential function is proposed to predict the nonlinear response of an epoxy matrix to any three-dimensional loading condition. The proposed potential function is a combination of the second and third invariants of the deviatoric stress tensor as well as the first invariant of the stress tensor, i.e. the hydrostatic stress. Series of tensile and shear constant-rate straining tests were performed on the epoxy resin specimens up to the fracture. The viscoplastic model parameters are derived from the experimental data, and the fracture patterns of the specimens under tensile and shear loadings are studied.

2. Constitutive equations

One of the versatile methods to describe the viscoplastic behavior of polymeric matrices is the flow plasticity theory. In this theory, it is assumed that the total applied strain can be decomposed into an elastic and an inelastic part. The inelastic stains are supposed to be present from the beginning of loading at all stress levels, thus a definition for the yield surface to detect the onset of inelasticity is not required. In order to determine the inelastic part of strain, a flow rule is used. The flow rule relates the inelastic deformation and a potential function that describes the loading condition. The constitutive equation to describe the triaxial stress-strain relation is considered as [4,22].

$$\{\sigma\} = [C]\left(\{\varepsilon\} - \{\varepsilon\}^I\right) \tag{1}$$

where $[C]$ is the stiffness matrix, and $\{\varepsilon\}^I$ is the inelastic part of the total strain $\{\varepsilon\}$. The rate of evolution of the inelastic strain is defined by a flow rule as in Eq. (2). The components of the inelastic strain rates are proportional to the derivative of a potential function f respect to the deviatoric stress components S_{ij}. In Eq. (2), $\dot{\lambda}$ is a positive scalar called the rate dependent hardening variable [3].

$$\dot{\varepsilon}^I_{ij} = \dot{\lambda}\frac{\partial f}{\partial S_{ij}} \tag{2}$$

The plastic behavior of various materials have been introduced by using different descriptions for the potential function f. As reviewed above, a potential function in terms of the second invariant of deviatoric stress J_2, to account for distortion, and the first invariant of stress I_1, to account for hydrostatic stress, has been used in the literature [5, 19and24]. In the present work, to include the effect of the load angle on the viscoplastic deformation, the third invariant of the deviatoric stress tensor J_3 is added to the potential function as shown in Eq. (3),

$$f = J_2^{3/2} - C\left(J_3 + I_1^3\right) \tag{3}$$

It is evident that the dimension of the potential function f in the above equation is the cubic stress. C is a constant that must be determined to preserve the convexity of the potential function under different loading conditions. The outward normal of the potential function represents the direction of the inelastic strain increment vector. A convex potential function ensures the inelastic strain increment vector to remain outward. By substituting the potential function of Eq. (3) into Eq. (2), and taking the derivative respect to time, the inelastic strain rate $\dot{\varepsilon}^I_{ij}$ becomes

$$\dot{\varepsilon}^I_{ij} = \dot{\lambda}\left[\frac{3}{2}S_{ij}\sqrt{J_2} - C\left(t'_{ij} + 3I_1^2\delta_{ij}\right)\right] \tag{4}$$

where δ_{ij} is the Kroneker delta and t'_{ij} is the derivative of J_3 with respect to the deviatoric stress components S_{ij} as

$$t'_{ij} = \frac{\partial J_3}{\partial S_{ij}} = S_{ik}S_{kj} - \frac{2}{3}J_2\delta_{ij} \tag{5}$$

To define the value of $\dot{\lambda}$, the principle of the equivalence of the inelastic work rate is employed. Using Eq. (3) and Eq. (4), the inelastic work rate $\dot{W}^I$ can be expressed by the following relation [25],

$$\dot{W}^I = \sigma_{ij}\dot{\varepsilon}^I_{ij} = \sigma_{ij}\dot{\lambda}\left[\frac{3}{2}S_{ij}\sqrt{J_2} - C\left(t'_{ij} + 3I_1^2\delta_{ij}\right)\right] = \sigma_e\dot{\varepsilon}^I_e \tag{6}$$

The effective stress σ_e and the effective inelastic strain rate $\dot{\varepsilon}^I_e$ are defined using a uniaxial stress state in which the relation between the potential function and the effective stress is obtained using Eq. (3) as follows

$$\sigma_e = \left(\frac{27f}{3\sqrt{3} - 29C}\right)^{1/3} \tag{7}$$

By replacing σ_e from Eq. (7) into Eq. (6), the relation for $\dot{\lambda}$ is resulted,

$$\dot{\lambda} = \frac{\dot{\varepsilon}^I_e}{\sqrt{3}\sigma_e^2} \tag{8}$$

In order to complete the above relation for $\dot{\lambda}$, the model developed by Bodner-Partom [26] is used for the effective inelastic strain rate in terms of σ_e, Z, a state variable, and D_0 and n that are two material constants.

$$\dot{\varepsilon}^I_e = \frac{2}{\sqrt{3}}D_0\exp\left[-\frac{1}{2}\left(\frac{Z}{\sigma_e}\right)^{2n}\right] \tag{9}$$

In the above model, n is a material constant that controls the rate dependency of the material, and D_0 is a constant of 10^6. By combining Eqs. (9) and (8) into Eq. (4), the final form of the inelastic strain rate is determined to be

$$\dot{\varepsilon}^I_{ij} = \frac{2D_0}{3\sigma_e^2}\exp\left[-\frac{1}{2}\left(\frac{Z}{\sigma_e}\right)^{2n}\right]\left[\frac{3}{2}S_{ij}\sqrt{J_2} - C\left(t'_{ij} + 3I_1^2\delta_{ij}\right)\right] \tag{10}$$

2.1. Determination of material constants

The state variable Z is a load history dependent parameter that expresses the hardening behavior of the material having a minimum initial value of Z_0 and a maximum value of Z_1. The differential equation for the rate of evolution of the state variable Z is defined as below [27].

$$\dot{Z} = q(Z_1 - Z)\,\dot{e}^I_e \tag{11}$$

where q is a material constant that controls the hardening rate, and $\dot{e}^I_e$ is the effective deviatoric inelastic strain rate to be obtained from the deviatoric inelastic strain rate $\dot{e}^I_{ij}$ and the mean inelastic strain rate $\dot{\varepsilon}^I_m$ [27].

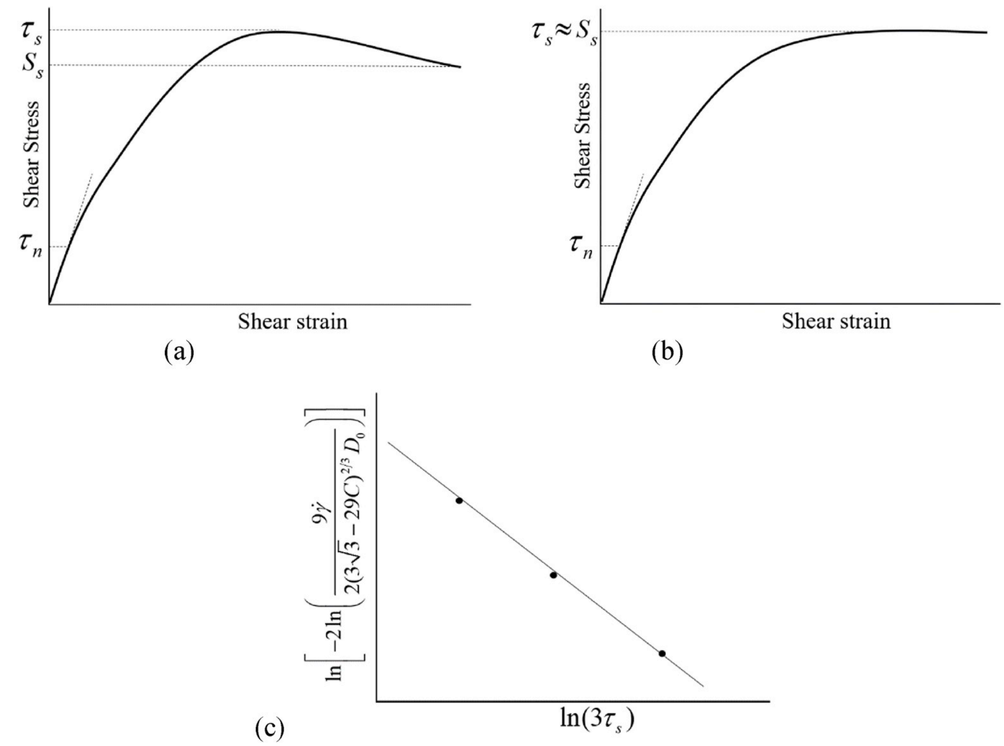

Fig. 1. Illustrations of (a) general shear stress-strain curve, (b) a special case for saturation stress, (c) correlation of material parameters.

$$\dot{e}^I_e = \sqrt{\frac{2}{3}\,\dot{e}^I_{ij}\,\dot{e}^I_{ij}} \qquad \text{in which } \dot{e}^I_{ij} = \dot{\varepsilon}^I_{ij} - \dot{\varepsilon}^I_m\,\delta_{ij} \tag{12}$$

In order to determine other material constants in Eq. (10) including Z_0, Z_1, n and q, a load case of shear stress is considered here for two reasons. First, the effects of hydrostatic stress are separated and second, polymers typically show more nonlinear responses under shear loading relative to normal loading. Under pure in-plane shear loading, Eq. (10) is simplified as follows

$$2\dot{\varepsilon}^I_{12} = \dot{\gamma}^I = \frac{2}{9}D_0 \exp\left[-\frac{1}{2}\left(\frac{(3\sqrt{3}-29C)^{1/3}Z}{3\tau}\right)^{2n}\right]\left(3\sqrt{3}-29C\right)^{2/3} \tag{13}$$

In a constant-rate shear test, the shear stress increases with the strain up to the saturation region where it approaches a plateau constant saturation shear stress τ_s, illustrated in Fig. 1(a) and (b). In the saturation region, the elastic strain remains constant and thus the inelastic strain rate is equal to the total applied shear strain rate $\dot{\gamma}$. Two types of shear stress-strain curve may be observed in practice, the saturation stress τ_s may be higher than, Fig. 1(a), or almost equal to the ultimate shear strength S_s, Fig. 1(b). By rearranging Eq. (13) and twice taking the natural logarithm of both sides, it leads to

$$\ln\left[-2\ln\left(\frac{9\dot{\gamma}}{2\left(3\sqrt{3}-29C\right)^{2/3}D_0}\right)\right] = 2n\ln\left[\left(3\sqrt{3}-29C\right)^{1/3}Z_1\right] - 2n\ln[3\tau_s] \tag{14}$$

The unknown material constants in Eq. (14) are found through some sets of shear stress-strain tests at different constant strain rates. In these tests, for each shear strain rate $\dot{\gamma}$ applied to the specimen, the saturation stress τ_s is obtained and the data point of $(\tau_s, \dot{\gamma})$ is used in a graph of Eq. (14) as shown in Fig. 1(c). By using a least square analysis, the slope $-2n$ and the intercept $2n\ln[(3\sqrt{3}-29C)^{1/3}Z_1]$ of the fitted line will be resulted.

To specify the value of Z_0, Eq. (13) is rearranged as follows

$$Z_0 = \frac{3\tau_n}{\left(3\sqrt{3}-29C\right)^{1/3}}\left[-2\ln\left(\frac{9\dot{\gamma}^I}{2\left(3\sqrt{3}-29C\right)^{2/3}D_0}\right)\right]^{1/2n} \tag{15}$$

where τ_n is the shear stress level at the point of deviation from linear extrapolation, illustrated in Fig. 1(a). At this point, the value of Z approaches Z_0 for which the value of the inelastic shear strain rate $\dot{\gamma}^I$ is approximated as one hundredth of the applied shear strain rate $\dot{\gamma}$ [23]. To specify the value of q in the case of pure shear condition, Eq. (11) is integrated between Z_0 and Z_1 to obtain q in terms of γ^I the inelastic shear strain.

$$Z = Z_1 - (Z - Z_0)\exp\left(\frac{-q}{\sqrt{3}}\gamma^I\right) \tag{16}$$

At saturation, the value of Z approaches Z_1 and thus the exponential term must vanish. In order to avoid singularity, the following small value is approximated for the exponential term at the saturation inelastic shear strain γ^I_s

$$\exp\left(\frac{-q}{\sqrt{3}}\gamma^I_s\right) = 0.01 \tag{17}$$

Through the above relation, the value of q is obtained. The parameter C must be chosen from within an acceptable interval to preserve the convexity of the potential function. The potential function is convex if and only if its Hessian matrix H is positive semi-definite, or in other words if and only if all three fundamental invariants of its Hessian matrix are positive or zero. The Hessian matrix of the potential function has the following definition in which $i,j = 1,2,3$ and σ_i are the principal stresses.

$$H_{ij} = \frac{\partial^2 f}{\partial\sigma_i\partial\sigma_j} \tag{18}$$

2.2. Numerical solution

Equation (10) is a nonlinear implicit differential equation between

Table 1
Specifications of the epoxy resin.

	Mixing ratio (by weight)	Density at 25 °C (g/cm^3)	Viscosity at 25 °C (mPa.s)	Pot life at 25 °C (min)	Gelation time at 25 °C (hr)
Resin	100	1.17	2850	–	–
Hardener	30	0.96	10	160	6

the stress and strain components. This equation cannot be solved analytically to obtain an exact solution, but may be solved numerically. To preserve the stability of the differential equation solution, fourth-order Runge-Kutta method is used in this work. The incremental form of Eq. (10) is obtained by rearranging it as below for time step $m+1$ in terms of the previous time step m,

$$\Delta\varepsilon^{I}_{ij}m+1 = \frac{2D_0}{3\sigma_{e\ m}{}^2}\exp\left[-\frac{1}{2}\left(\frac{Z_m}{\sigma_{e\ m}}\right)^{2n}\right]\left[\frac{3}{2}S_{ij\ m}\sqrt{J_{2\ m}} - C\left(t'_{ij\ m} + 3I_{1\ m}{}^2\delta_{ij}\right)\right]\Delta t \tag{19}$$

At the first time step, $m = 0$, the value of Z is as Z_0, and the values of σ_{ij} are calculated at a very small initial strain in the order of 10^{-5} mm/mm as the starting value. In the next time steps, Z is independently calculated using Eq. (11), and the values of σ_e, S_{ij}, t'_{ij}, I_1 and J_2 are calculated from σ_{ij}. The total strain is calculated from $\varepsilon_{ij\ m+1} = \varepsilon_{ij\ m} + \dot{\varepsilon}_{ij\ m+1}\Delta t$ where $\dot{\varepsilon}_{ij\ m+1}$ is the applied input strain rate. At any time step, all of the terms in Eq. (19) are calculated at four increments, and the results of each increment are used as the input for the next one which ensures the convergence.

3. Materials and methods

An industrial epoxy resin from Epolam was selected for the experimental part of this work consisting of resin, Epolam 2017, and hardener, Epolam 2018. The physical specifications of this room-temperature curing resin are detailed in Table 1. The mixture of the resin and hardener was degassed to minimize blending process air bubbles, and then cured at room temperature of 25 °C in two different size rectangular molds having a thickness of 5 mm, shown in Fig. 2(a). A group of 70 × 75 mm almost square specimens was prepared for the shear tests, and a group of 35 × 250 mm rectangular specimens for the uniaxial tensile tests, see Fig. 2(b).

3.1. Experimental set-up

Tensile and shear tests were performed based on ASTM standards D3039 and D7078, respectively, using a universal testing machine. A pair of special fixtures was designed capable of being mounted in the hydraulic grips of the tension machine to apply in-plane shear deformation to the resin specimens, Fig. 3. The pair of fixtures is a newly

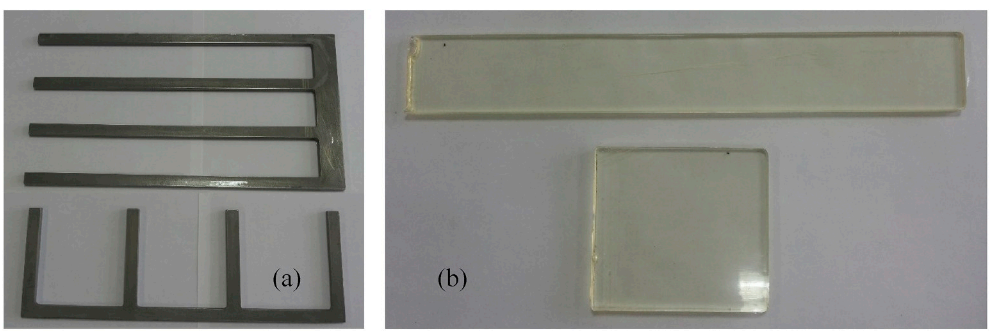

Fig. 2. (a) Metal rectangular molds, (b) epoxy resin specimens for tensile and shear tests.

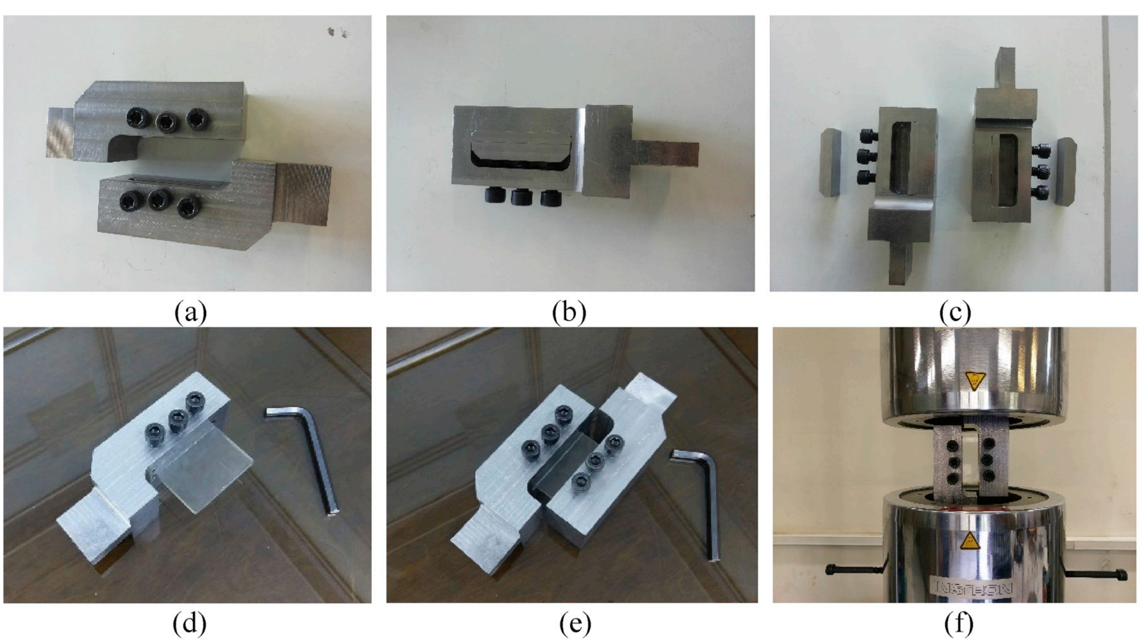

Fig. 3. (a)–(e) Fixtures newly designed for shear deformation tests, (f) fixtures in tension machine.

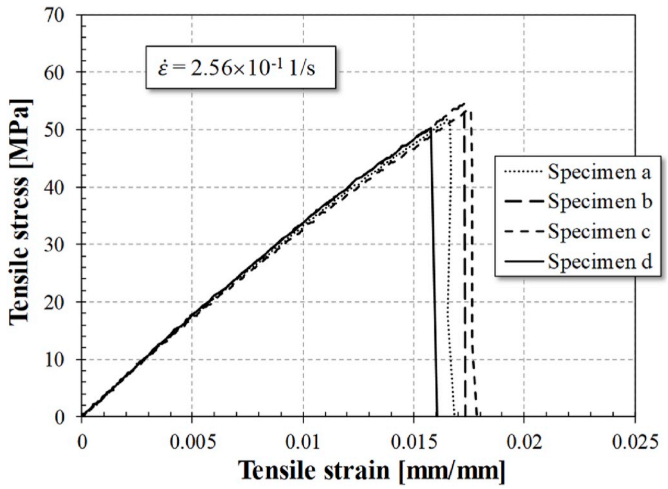

Fig. 4. Tensile stress-strain curves at 2000 mm/min displacement rate.

designed version of those presented in ASTM D7078 aimed to remove weaknesses of the previous version. Automatic certain alignment of the specimen and the simplicity of mounting into the testing machine grips are the advantages of the present design.

A square resin specimen was installed into the pair of fixtures, and a constant-rate displacement up to 3240 mm/min was applied to the lower fixture, Fig. 3(f). In the present work, five different displacement rates were used for both tensile and shear tests from a quasi static displacement rate up to the maximum velocity limit of the testing machine which were 2, 20, 200, 2000 and 3240 mm/min. Despite of the similar applied displacement rates in tension and shear rests, the rates of the normal and shear strains were not similar due to different dimensions of the specimens.

4. Results and discussion

4.1. Experimental results

The experimental part of this work is aimed to characterize the viscoplastic properties as well as to verify the viscoplastic model for the resin behavior.

4.1.1. Tensile stress-strain behavior

The tension specimens having a gage length of 130 mm were tested under constant strain rates of 2.56×10^{-4}, 2.56×10^{-3}, 2.56×10^{-2}, 2.56×10^{-1} and 4.15×10^{-1} 1/s corresponding to the displacement rates of 2, 20, 200, 2000 and 3240 mm/min, respectively. Each constant-rate tensile strain test was carried out four times in order to investigate the repeatability of data. The experimental results for four tensile tests at 2000 mm/min are presented in Fig. 4. It is observed that the tensile stress-strain curve of the resin has a slight curvature being repeated very well and ending with a sudden fracture. The strength at the breaking point has a reasonable scatter. It is known that the breaking point of the specimen depends on the size, position and distribution of microscopic initial cracks on the edges of the specimen. A similar scatter is also observed in the tensile tests performed at the other strain rates. Fig. 4 shows that the initial tensile modulus has almost no scatter between the repetitions of the test, less than 0.5%, but for the tensile strength a maximum of 5% scatter is observed between the average and the highest and lowest experimental values. For the material characterization, the strength of specimens tested under identical strain rates were averaged to obtain the nominal strength in each strain rate.

4.1.1.1. Tensile fracture behavior. The specimens tested at constant rates of 20 and 2000 mm/min are shown in Fig. 5(a) and (b) for instance. The fracture patterns show that the cracking starts and continues normal to the load direction within the gage length of the specimen. These are indications of the brittle behavior of the resin which is apparently sensitive to the normal stress component instead of the shear, and also sensitive to the average stress which is larger within the gauge length rather than in the grips. This observation also justifies the application of a rectangular shape for the specimens in this work according to ASTM D3039, instead of a dumbbell shape. In most of the specimens, the crack propagates with a deviation from the initial crack line. All stress components within the crack zone, especially the component parallel to the crack line called T-stress, significantly affect the direction of the crack propagation [28]. The initial crack growth normal to the load direction reduces the load-carrying part of the specimen cross section, which induces an eccentricity of the applied axial load, and thus a bending moment. Therefore, a combined bending and tensile loading mode, instead of a pure tensile, is expected by the increase of the initial crack

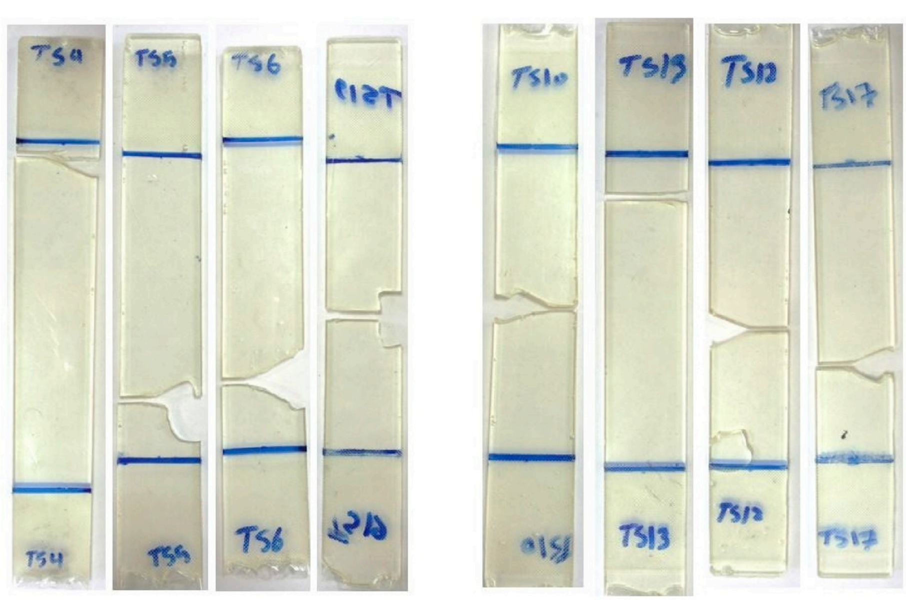

(a) (b)

Fig. 5. Fracture patterns in tensile specimens tested at (a) 2.56×10^{-3} 1/s and (b) 2.56×10^{-1} 1/s.

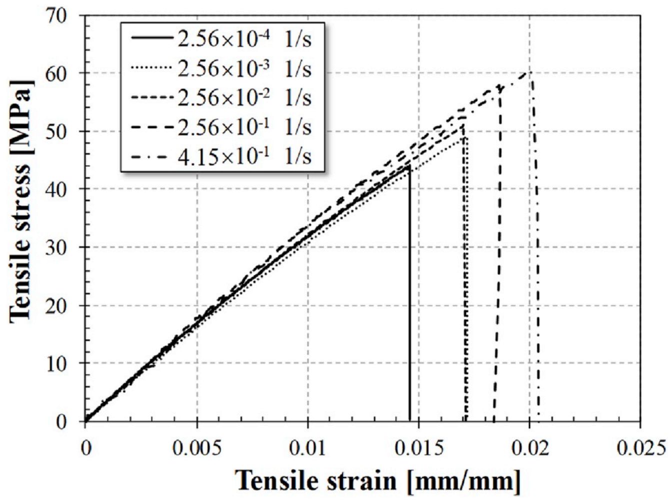

Fig. 6. Results of tensile tests performed at various constant strain rates.

length.

Typically, a fracture criterion like maximum tangential strain [29] and minimum strain energy density [30], is used to explain the crack trajectory. In these criteria, the parameter that mostly provides a good prediction of the crack trajectory is T-stress. For any material, the value of T-stress changes from negative to positive value when there is a variation in loading mode and specimen geometry. When T-stress is less than its critical value, or the crack zone is small, the crack will propagate along its initial crack line. But afterwards, when T-stress surpasses its critical value or there is a large crack zone, the crack propagates out of its initial direction at an angle even up to 90° [29,30], see Fig. 5(a).

4.1.1.2. Rate-dependency of the tensile stiffness and strength. A comparison between the experimental tensile stress-strain curves at various constant strain rates is presented in Fig. 6. It is observed that the stress-strain curve at any strain rate consists of a linear part followed by a slightly nonlinear part leading to a tensile strength. At higher strain rates, the specimens show less nonlinearity than that at lower strain rates, and the curve tends to a brittle-like straight line. It is noted that within the range of the strains applied to the specimens up to the breakage, less than 0.02 mm/mm, the difference of the true strain and engineering strain is not notable, and thus the curvature observed in these tests is not due to nonlinear geometry for large strains. On the other hand, the transverse strains are thus so small that the change in the cross section may be ignored. On this basis, the initial cross-sectional area of the specimen was used to calculate the axial engineering stress which is almost the same as true stress. This is the case not only for the tensile tests but also for the shear tests to be presented in the next sections.

The tensile stress-strain curves at various strain rates are compared in two aspects, the rate-dependency of stiffness and the rate-dependency of strength. The overall slope of the stress-strain curve increases with the strain rate, so that the initial Young's modulus increases by about 6.9% for the strain rates from 2.56×10^{-4} to 4.15×10^{-1} 1/s. This is presented in the graphs of Fig. 7 where both normal and logarithmic scales are used for the horizontal strain rate axis. Within about three decades of

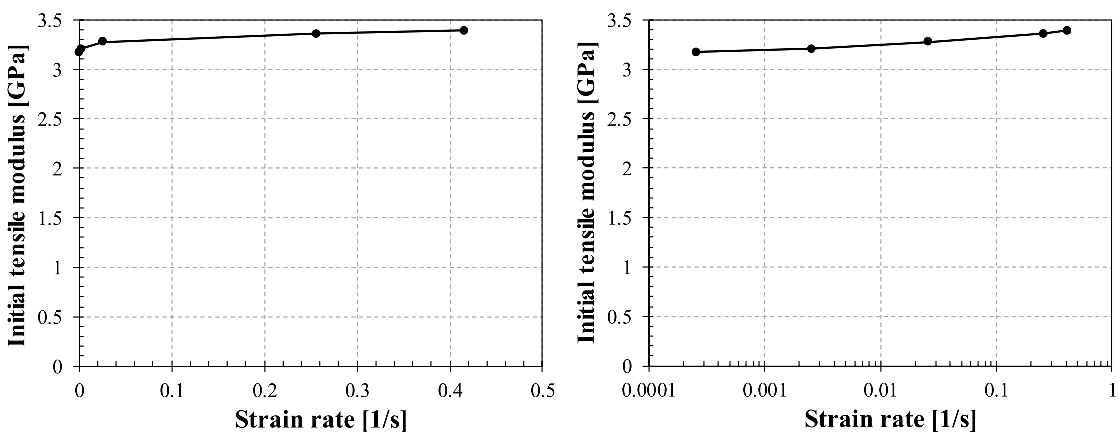

Fig. 7. Rate dependency of the initial Young's modulus.

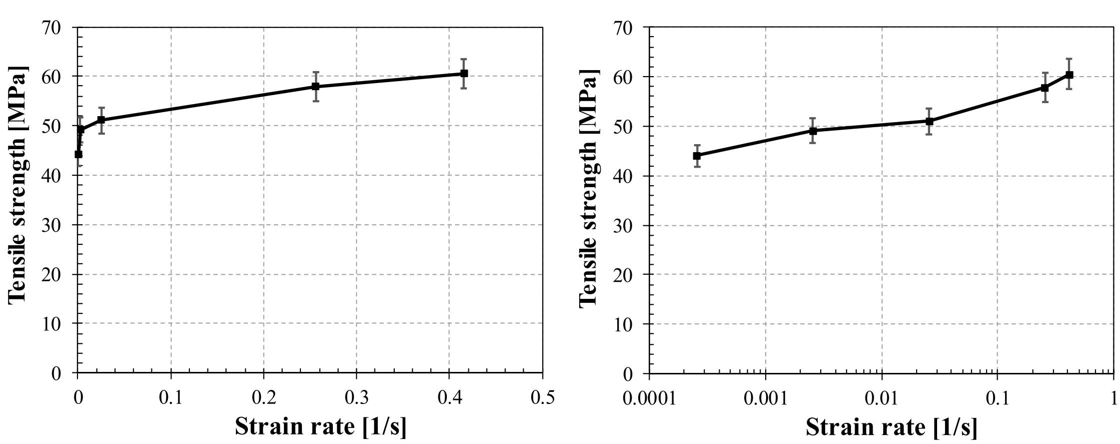

Fig. 8. Rate dependency of the tensile strength.

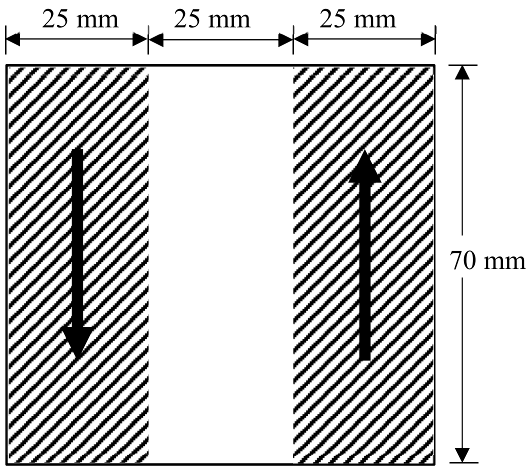

Fig. 9. Dimensions of a shear test specimen.

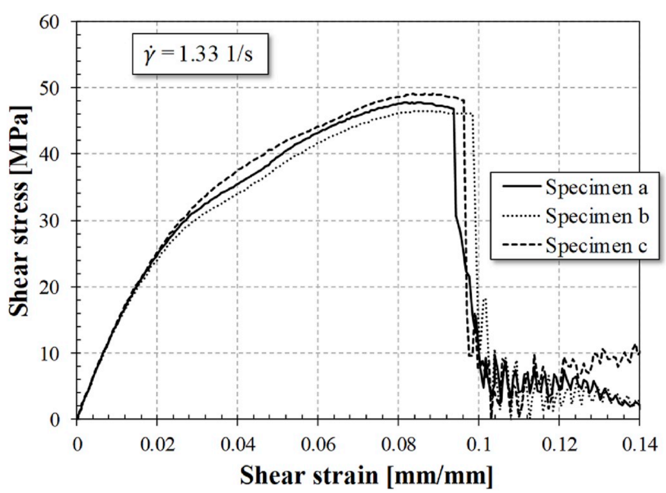

Fig. 10. Shear stress-strain curves at 2000 mm/min displacement rate.

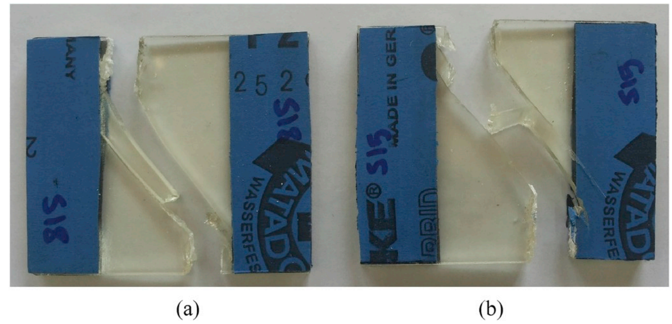

Fig. 11. Fracture patterns in shear specimens tested at (a) 0.133 1/s and (b) 1.33 1/s.

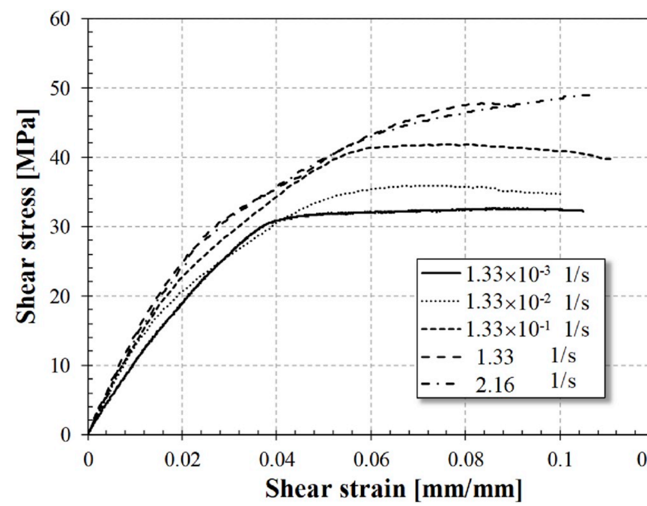

Fig. 12. Results of simple shear tests performed at various constant strain rates.

the strain rate, which is the practical range for the tension machine, an increase of 6.9% for the modulus is significant. The increase of the modulus of the resin with stain rate is due to the viscoelastic behavior of the material. On the other hand, the tensile strength increases by about 37.5% over the same range of the strain rate, see Fig. 8. This shows a substantial increase of the tensile strength of the resin with the increase of the strain rate. The experimental scatter of the strength is shown by error bars in Fig. 8.

4.1.2. Shear stress-strain behavior

The gage part of the shear test specimens having dimensions of 25 × 70 mm is shown in Fig. 9 as the middle unhatched one-third of the specimen which goes under pure shear loading. The shear strain was applied to the specimens at the constant rates of 1.33×10^{-3}, 1.33×10^{-2}, 1.33×10^{-1}, 1.33 and 2.16 1/s corresponding to the displacement rates of 2, 20, 200, 2000 and 3240 mm/min. Each constant-rate shear strain test was carried out three times. The experimental data for the shear tests at 2000 mm/min displacement rate are shown in Fig. 10. In comparison with the tensile tests, a significant nonlinear stress-strain behavior is observed for the resin under shear loading. The repeatability of the results is acceptable for shear tests at all strain rates. Fig. 10 shows that the initial shear modulus has almost no scatter between the repetitions of the test, less than 1%, but for the shear strength a maximum of 6% scatter is observed between the average and the highest and lowest experimental values.

4.1.2.1. Shear fracture behavior. Two samples of the specimens tested at 200 and 2000 mm/min are shown in Fig. 11. In an effort to minimize the slippage of the specimen and the stress concentration, sandpaper tabs were used on the specimen sides in the fixtures. Oblique fracture patterns through the middle of these specimens show that the crack occurs in a plane 45° from the plane of the applied shear stress. Similar fracture patterns are observed in all specimens failed in the gage part. This is a basic indication of the brittle behavior of the resin whose atomic bonds may be broken under a normal tensile stress. Further, the final stepwise part of the stress-strain curves in Fig. 10 is due to the parallel multi-cracking of the specimens shown in Fig. 11. In addition, it is noticed that after initiation and growth of the cracks along 45° planes, the cracking stops at the fixtures and continues parallel to the fixtures.

4.1.2.2. Rate-dependency of the shear stiffness and strength. The experimental data for shear stress-strain curves at different displacement rates are compared in Fig. 12. Under shear loading, the nonlinear rate-dependent response of the resin is significantly more evident than that under tensile loading, even at low strain rates. The nonlinear response starts at low strains of about 0.01 mm/mm, and grows with straining as well as with the strain rate. The stress-strain curves approach a plateau region in the final part of the shear tests before the breaking point. This implies that the saturation stress converges the shear strength of the material, as illustrated in Fig. 1(b). The rate dependency of the initial shear modulus is shown in the graphs of Fig. 13. The initial shear modulus increases about 12% over three decades of the shear strain rate from 1.33×10^{-3} to 2.16 1/s. On the other hand, the shear strength also increases about 51.7% over the same decades of the strain rate shown in Fig. 14. In this figure, the experimental scatter of the strength is shown

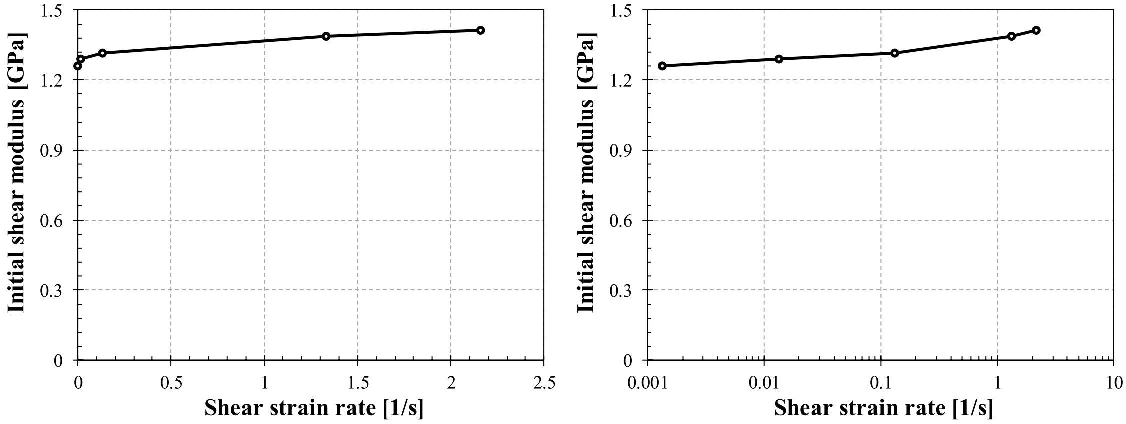

Fig. 13. Rate dependency of the initial shear modulus.

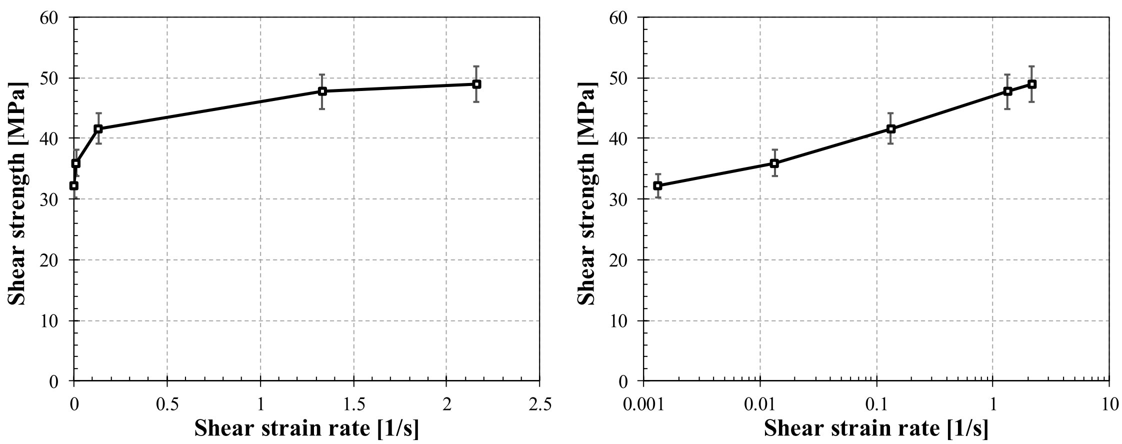

Fig. 14. Rate dependency of the shear strength.

Table 2
Experimental results of simple shear tests.

Shear strain rate, $\dot{\gamma}$[1/s]	Initial shear modulus [MPa]	τ_n[MPa]	τ_s[MPa]
0.001333	1259	14.0	32.2
0.01333	1288	14.4	35.9
0.1333	1315	15.6	41.6
1.333	1389	17.0	47.7
2.16	1411	21.0	48.8

by error bars.

4.2. Material model characterization results

In order to obtain the model constants, several material properties including nonlinear stress level τ_n, saturation stress τ_s and initial shear modulus are extracted from shear stress-strain curves at various strain rates summarized in Table 2. The parameters τ_s and $\dot{\gamma}$ are used in Eq. (14) to draw the graph of Fig. 15 which results in n and Z_1 through linear regression. It is found that the bounds on C to preserve the convexity of the potential function in Eq. (3), are $[-105, 0.03]$ for uniaxial loading condition and $[-1.2, 1.2]$ for shear loading condition. Here, a value of $C=-1$ is assumed in the model. On the other hand, τ_n, $\dot{\gamma}$ and n are used in Eq. (15) to obtain Z_0. Further, the initial modulus is used to estimate the unloading saturation inelastic shear strain γ_s^I to be used in Eq. (17) to obtain q. The results of the above calculations are presented in Table 3.

The initial Young's moduli are also extracted for tensile tests carried out at various strain rates and shown in Table 4. For higher strain rates,

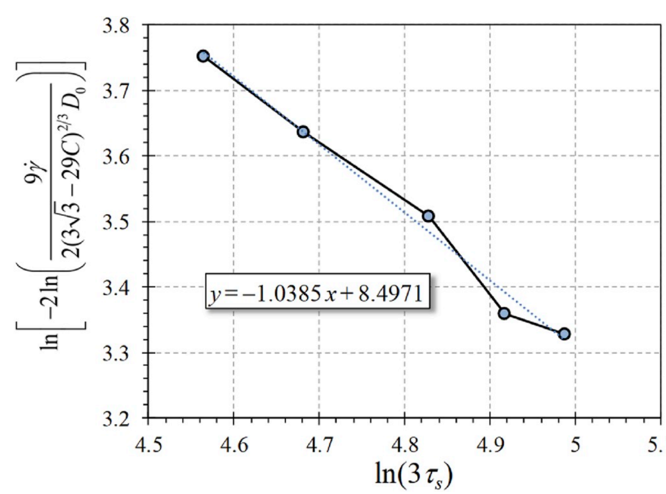

Fig. 15. Correlation of the model parameters to obtain n, Z_1.

elastic moduli are obtained from a combination of shear tests and

Table 3
Model parameters for the epoxy resin.

D_0[1/s]	Z_0[MPa]	Z_1[MPa]	n	q	C
10^6	627.2	1105.2	0.52	80.1	−1

Table 4
Experimental results of tensile tests.

Strain rate [1/s]	Initial Young's modulus [MPa]
0.000256	3168
0.00256	3200
0.0256	3210
0.256	3358
0.415	3391

extrapolations. On the basis of the initial Young's and shear moduli at different strain rates presented in Tables 2 and 4, the Poisson's ratio for the resin is obtained to be about 0.26 with a deviation of ± 0.08. Therefore, an assumption of constant Poisson's ratio for the resin is justified.

4.3. Model prediction results

After completing the material characterization and obtaining all model constants as in Table 3, the present viscoplastic model is validated by predicting the responses of the resin to the tensile and shear loadings. For instance, constant-rate tensile and shear strains are applied in the incremental Eq. (19) and the stress is calculated. The model predictions are compared with the experimental data obtained in the present work shown in Figs. 16 and 17. The predicted results show a good agreement with the experimental tensile and shear responses for all strain rates considered. Specifically, the rate-dependent initial moduli and the ultimate strengths for the tensile and shear tests are well predicted. The significant nonlinearity in the shear behavior, respect to the tensile behavior, is predicted very well at different strain rates.

4.3.1. Effect of model parameter C

To further investigate the effect of parameter C on the model prediction, a value of $C = 0$ from within the acceptable convexity interval is considered in calculating the shear stress-strain curve at 1.33 1/s strain rate. Fig. 18 presents the experimental data compared with the model predictions using both $C = 0$ and $C = -1$. As can be seen, when the parameter C vanishes in the stress calculations, the shear stress is significantly underestimated. Also the parameter C, in addition to preserve the convexity of the potential function, makes a good correlation between theoretical and experimental results.

4.3.2. Comparison with Goldberg's model

One of the constitutive models to describe the rate-dependent mechanical behavior of the polymers has been Goldberg's model [23]. The potential function in Goldberg's model is defined as in Eq. (20) which results in Eq. (21) for the inelastic strain components as follows

$$f = J_2^{1/2} + \alpha\,\sigma_{kk} \tag{20}$$

$$\dot{\varepsilon}_{ij}^{I} = 2D_0 \exp\left[-\frac{1}{2}\left(\frac{Z}{\sigma_e}\right)^{2n}\right]\left[\frac{S_{ij}}{2\sqrt{J_2}} + \alpha\delta_{ij}\right] \tag{21}$$

In the above relations, all characters are as explained for the constitutive model in Section 2, and α is a state variable introduced in Goldberg's model to account for the effect of the hydrostatic stress σ_{kk} [23]. In order to use this model to predict the behavior of our epoxy resin, the model constants are determined according to the procedure described in Ref. [23], see Table 5, where α_0 and α_1 are the minimum and maximum values of α.

The predictions of Goldberg's model and the present model are compared with the experimental data for tensile and shear loadings at various strain rates in Figs. 19 and 20. The resin behavior in tensile tests having a slight nonlinearity is well predicted by both constitutive models. However, the difference of Goldberg's model with the experimental data increases significantly for the nonlinear shear stress-strain curves. If the shear stress-strain curve is divided into three regions of the initial linear elastic part, the nonlinear middle part and the final plateau at saturation stress, the largest deviation of Goldberg's model occurs in the middle part of the curve. This is mainly due to the underestimation of the inelastic strain in Goldberg's model which results in a linear behavior up to about the saturation stress.

5. Conclusion

In this work, a new viscoplastic model was developed to predict the nonlinear rate-dependent mechanical behavior of an epoxy resin. The presented model is based on a potential function that is made a combination of the second and third invariants of deviatoric stress tensor as well as the first invariant of stress tensor. A set of tensile and shear tests at various constant strain rates were performed to investigate the rate dependency of the resin and to derive the model parameters. Under shear loading, the nonlinearity of the stress-strain curve of the resin is significantly more evident than that under tensile loading, even at low strain rates. The initial modulus and strength of the resin increase with the strain rate both under tensile and shear loadings, however that is more significant under shear loading. Also, the fracture patterns for the tensile and shear specimens were studied. On the other hand, the

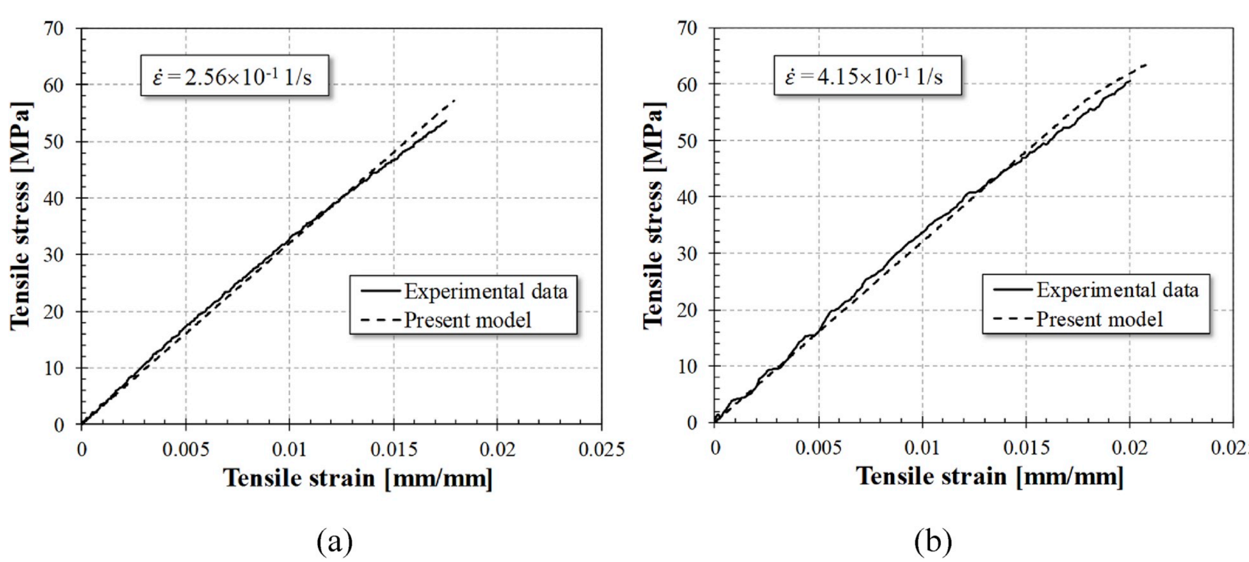

Fig. 16. Present model predictions versus experimental tensile test results.

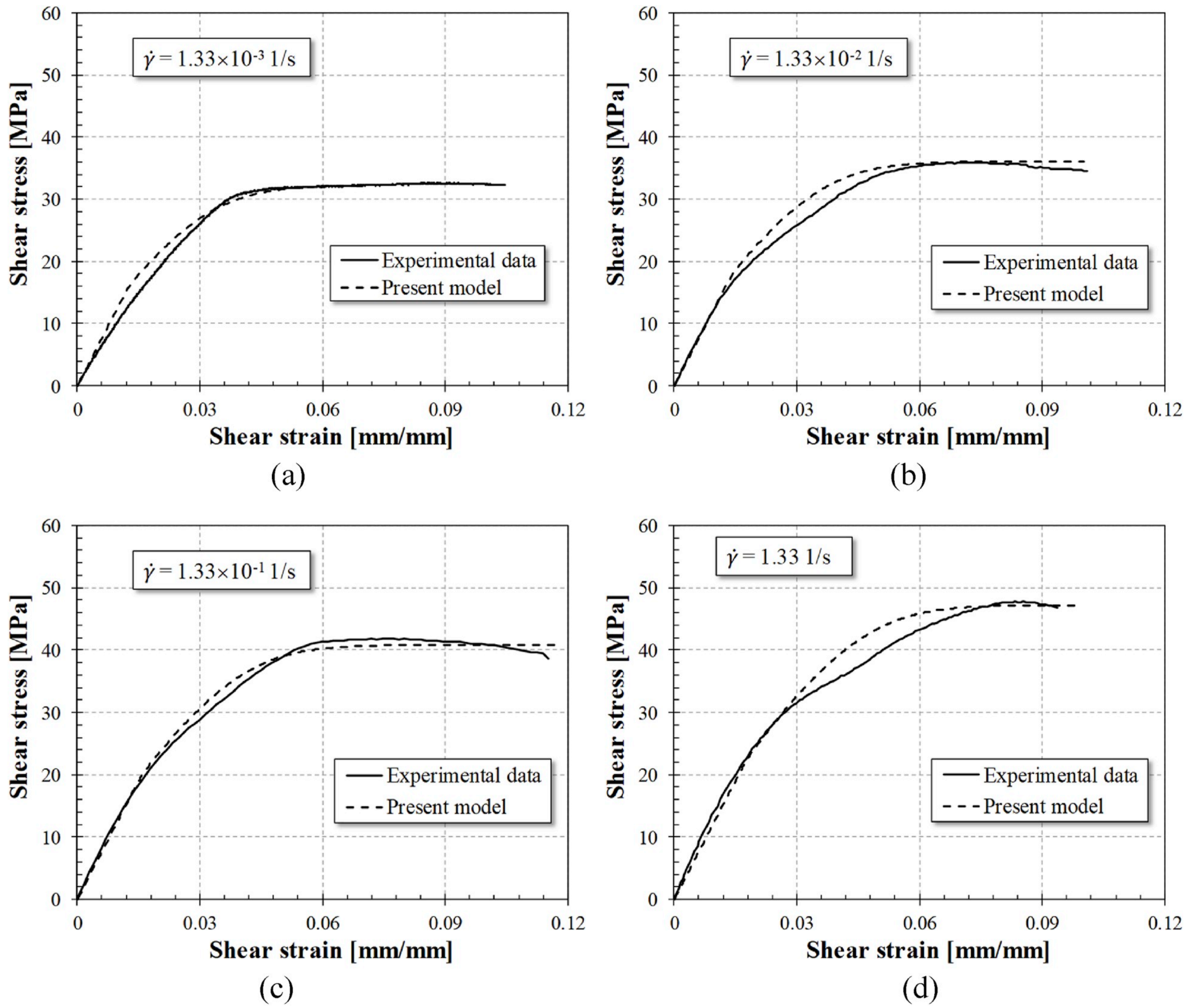

Fig. 17. Present model predictions versus experimental shear test results.

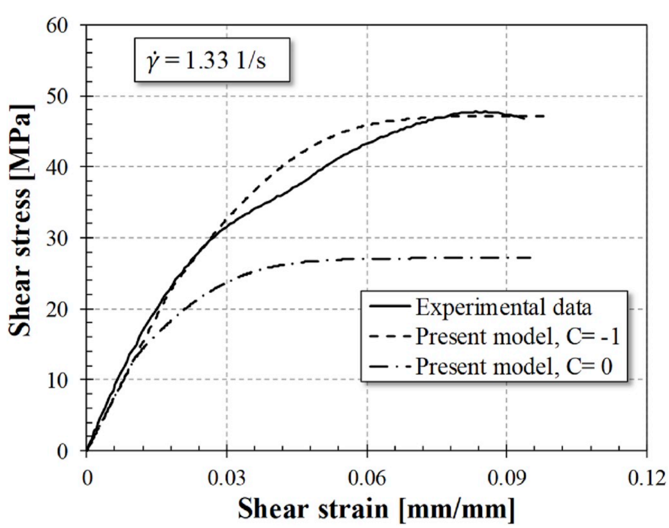

Fig. 18. Effect of parameter C on the model prediction.

Table 5
Goldberg's model constants for our resin.

D_0(1/s)	Z_0(MPa)	Z_1(MPa)	q	n	α_0	α_1
10^6	1703.0	1988.8	110.0	0.53	−0.135	0.0753

proposed viscoplastic model was successfully validated by predicting the responses of the resin to the tensile and shear loadings. Furthermore, by using our experimental data, it was shown that Goldberg's model may predict the resin response with a significant difference.

Data availability

The raw data required to reproduce these findings cannot be shared at this time as the data also forms part of an ongoing study. The processed data required to reproduce these findings cannot be shared at this time as the data also forms part of an ongoing study.

Declaration of competing interest

The authors declare that they have no known competing financial interests or personal relationships that could have appeared to influence the work reported in this paper.

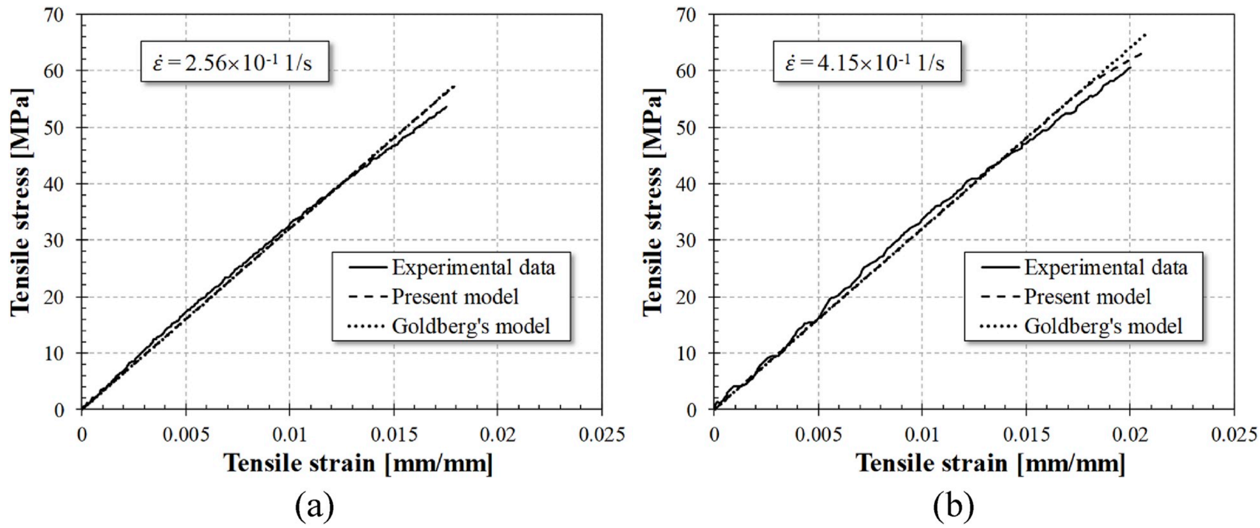

Fig. 19. Comparison of present model with Goldberg's model predictions for tensile loading.

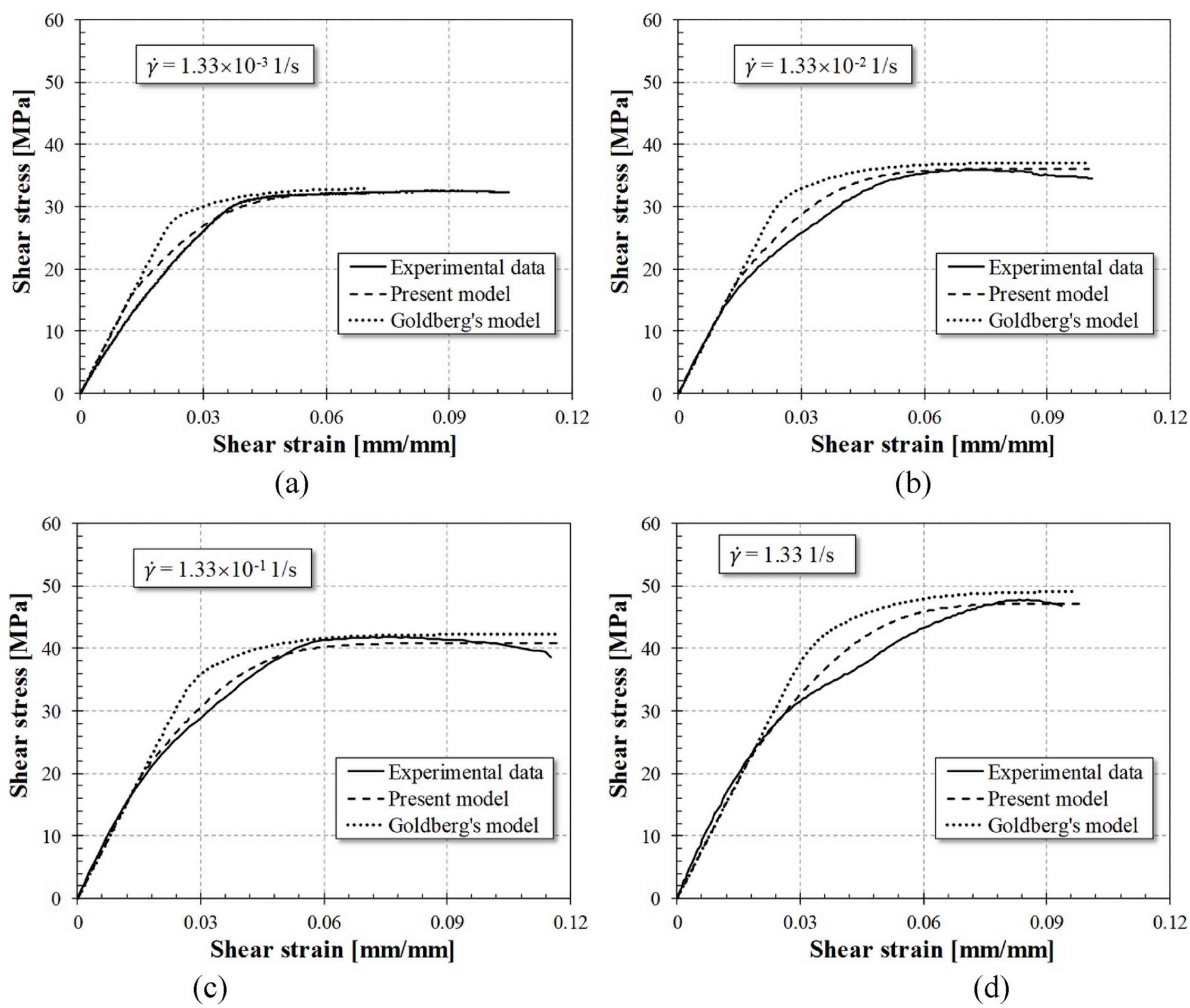

Fig. 20. Comparison of present model with Goldberg's model predictions for shear loading.

CRediT authorship contribution statement

Ehsan Shafiei: Conceptualization, Methodology, Software, Validation, Investigation, Data curation, Resources, Writing - original draft. **Mehdi Saeed Kiasat:** Supervision, Writing - review & editing, Visualization, Project administration.

References

[1] N. Taniguchi, T. Nishiwaki, H. Kawada, Tensile strength of unidirectional CFRP laminate under high strain rate, Adv. Compos. Mater. 16 (2007) 167–180, https://doi.org/10.1163/156855107780918937.

[2] F. Fereshteh-Saniee, G.H. Majzoobi, M. Bahrami, An experimental study on the behavior of glass–epoxy composite at low strain rates, J. Mater. Process. Technol. 162–163 (2005) 39–45, https://doi.org/10.1016/j.jmatprotec.2005.02.011.

[3] S.V. Thiruppukuzhi, C.T. Sun, Models for the strain-rate-dependent behavior of polymer composites, Compos. Sci. Technol. 61 (2001) 1–12, https://doi.org/10.1016/S0266-3538(00)00133-0.

[4] M.M. Shokrieh, R. Mosalmani, M.J. Omidi, A strain-rate dependent micromechanical constitutive model for glass/epoxy composites, Compos. Struct. 121 (2015) 37–45, https://doi.org/10.1016/j.compstruct.2014.10.035.

[5] A.R. Melro, P.P. Camanho, F.M. Andrade Pires, S.T. Pinho, Micromechanical analysis of polymer composites reinforced by unidirectional fibres: Part I – constitutive modelling, Int. J. Solid Struct. 50 (2013) 1897–1905, https://doi.org/10.1016/j.ijsolstr.2013.02.009.

[6] W. Van Paepegem, I. De Baere, J. Degrieck, Modelling the nonlinear shear stress–strain response of glass fibre-reinforced composites. Part I: experimental results, Compos. Sci. Technol. 66 (2006) 1455–1464, https://doi.org/10.1016/j.compscitech.2005.04.014.

[7] J. Tsai, C.T. Sun, Constitutive model for high strain rate response of polymeric composites, Compos. Sci. Technol. 62 (2002) 1289–1297, https://doi.org/10.1016/S0266-3538(02)00064-7.

[8] J.F. Chen, E.V. Morozov, A consistency elasto-viscoplastic damage model for progressive failure analysis of composite laminates subjected to various strain rate loadings, Compos. Struct. 148 (2016) 224–235, https://doi.org/10.1016/j.compstruct.2016.03.049.

[9] H. Ryou, K. Chung, Development of viscoelastic/rate-sensitive-plastic constitutive law for fiber-reinforced composites and its applications Part II: numerical formulation and verification, Compos. Sci. Technol. 69 (2009) 292–299, https://doi.org/10.1016/j.compscitech.2007.06.025.

[10] H. Ryou, K. Chung, W.R. Yu, Constitutive modeling of woven composites considering asymmetric/anisotropic, rate dependent, and nonlinear behavior, Composites Part A 38 (2007) 2500–2510, https://doi.org/10.1016/j.compositesa.2007.08.003.

[11] D. Cai, G. Zhou, X. Wang, C. Li, Ji Deng, Experimental investigation on mechanical properties of unidirectional and woven fabric glass/epoxy composites under off-axis tensile loading, Polym. Test. 58 (2017) 142–152, https://doi.org/10.1016/j.polymertesting.2016.12.023.

[12] L. Xing, K.L. Reifsnider, Progressive failure modeling for dynamic loading of woven composites, Appl. Compos. Mater. 15 (2008) 1–11, https://doi.org/10.1007/s10443-008-9053-7.

[13] T. Matsuda, Y. Nimiya, N. Ohno, M. Tokuda, Elastic–viscoplastic behavior of plain-woven GFRP laminates: homogenization using a reduced domain of analysis, Compos. Struct. 79 (2007) 493–500, https://doi.org/10.1016/j.compstruct.2006.02.008.

[14] X. Poulain, A.A. Benzerga, R.K. Goldberg, Finite-strain elasto-viscoplastic behavior of an epoxy resin: experiments and modeling in the glassy regime, Int. J. Plast. 62 (2014) 138–161, https://doi.org/10.1016/j.ijplas.2014.07.002.

[15] B. Farrokh, A.S. Khan, A strain rate dependent yield criterion for isotropic polymers: low to high rates of loading, Eur. J. Mech. Solid. 29 (2010) 274–282, https://doi.org/10.1016/j.euromechsol.2009.08.004.

[16] E.S. Shin, K.D. Pae, Effects of hydrostatic pressure on the torsional shear behavior of graphite/epoxy composites, J. Compos. Mater. 26 (1992) 462–485, 10.1177%2F002199839202600401.

[17] M.S. Kiasat, G.Q. Zhang, L.J. Ernst, G. Wisse, Creep behavior of a molding compound and its effect on packaging process stresses, in: Proceedings of 51st Electronic Components and Technology Conference (ECTC2001), Orlando, May, 2001, pp. 931–938, https://doi.org/10.1109/ECTC.2001.927907.

[18] M. Rezai Sangtabi, M.S. Kiasat, Long-term viscoelastic properties of an adhesive and molding compound, characterization and modeling, Polymer 116 (2017) 204–217, https://doi.org/10.1016/j.polymer.2017.03.074.

[19] B.T. Werner, I.M. Daniel, Characterization and modeling of polymeric matrix under multi-axial static and dynamic loading, Compos. Sci. Technol. 102 (2014) 113–119, https://doi.org/10.1016/j.compscitech.2014.07.025.

[20] G.M. Vyas, S.T. Pinho, P. Robinson, Constitutive modelling of fibre-reinforced composites with unidirectional plies using a plasticity-based approach, Compos. Sci. Technol. 71 (2011) 1068–1074, https://doi.org/10.1016/j.compscitech.2011.03.009.

[21] D.C. Drucker, W. Prager, Soil mechanics and plastic analysis or limit design, Q. Appl. Math. 10 (1952) 157–165.

[22] X. Bai, M.A. Bessa, A.R. Melro, P.P. Camanho, L. Guo, W.K. Liu, High-fidelity micro-scale modeling of the thermo-visco-plastic behavior of carbon fiber polymer matrix composites, Compos. Struct. 134 (2015) 132–141, https://doi.org/10.1016/j.compstruct.2015.08.047.

[23] R.K. Goldberg, G.D. Roberts, A. Gilat, Implementation of an associative flow rule including hydrostatic stress effects into the high strain rate deformation analysis of polymer matrix composites, J. Aero. Eng. 18 (1) (2005) 18–27, https://doi.org/10.1061/(ASCE)0893-1321(2005)18:1(18).

[24] S.Y. Hsu, T.J. Vogler, S. Kyriakides, Inelastic behavior of an AS4/PEEK compositeunder combined transverse compression and shear. Part II: modeling, Int. J. Plast. 15 (1999) 807–836, https://doi.org/10.1016/S0749-6419(99)00012-1.

[25] V.V. Vasiliev, E.V. Morozov, Advanced Mechanics of Composite Materials and Structural Elements, third ed., Elsevier Ltd, 2013.

[26] S.R. Bodner, Unified Plasticity for Engineering Applications, first ed., Springer US, 2002, p. 47.

[27] A.K. Miller, Unified Constitutive Equations for Creep and Plasticity, first ed., Elsevier Applied Science Publishers Ltd, 1987.

[28] O. Bouledroua, M. Hadj Meliani, G. Pluvinage, A review of T-stress calculation methods in fracture mechanics computation, Nat. Technol 8 (2016) 21–31.

[29] M.D. Wei, F. Dai, N.W. Xu, Y. Liu, T. Zhao, Fracture prediction of rocks under mode I and mode II loading using the generalized maximum tangential strain criterion, Eng. Fract. Mech. 186 (2017) 21–38, https://doi.org/10.1016/j.engfracmech.2017.09.026.

[30] Y. Wei, An extended strain energy density failure criterion by differentiating volumetric and distortional deformation, Int. J. Solid Struct. 49 (2012) 1117–1126, https://doi.org/10.1016/j.ijsolstr.2012.01.015.